Atmos. Chem. Phys. Discuss., 9, 3367–3399, 2009
www.atmos-chem-phys-discuss.net/9/3367/2009/

Atmospheric Chemistry and Physics Discussions

This discussion paper is/has been under review for the journal *Atmospheric Chemistry and Physics (ACP)*. Please refer to the corresponding final paper in *ACP* if available.

Cloud-type dependencies of MODIS and AMSR-E liquid water path differences

M. de la Torre Juárez[1], **B. H. Kahn**[1,2], **and E. J. Fetzer**[1]

[1]Jet Propulsion Laboratory/California Inst. of Technology, Pasadena, CA 91109–8099, USA
[2]Joint Institute for RegionalEarth System Science and Engineering, U.C.L.A., Los Angeles, CA, USA

Received: 17 November 2008 – Accepted: 23 December 2008 – Published: 2 February 2009

Correspondence to: M. de la Torre Juárez (mtj@jpl.nasa.gov)

Published by Copernicus Publications on behalf of the European Geosciences Union.

Abstract

Comparisons of cloud liquid water path (LWP) retrievals are presented from the Moderate Resolution Imaging Spectroradiometer (MODIS) and the Advanced Microwave Scanning Radiometer (AMSR-E) located aboard the Aqua spacecraft. LWP differences as a function of cloud top height, cloud fraction, cloud top temperature, LWP, cloud effective radius and cloud optical thickness are quantified in most geophysical conditions. The assumption of vertically homogeneous distributions of cloud water content in the MODIS LWP retrieval yields a slightly poorer agreement than the assumption of stratified cloud liquid water. Furthermore, for a fixed cloud top pressure, the cloud top temperature can lead to sign changes in the LWP difference. In general, AMSR-E LWP is larger than MODIS for small cloud fractions, low values of LWP, and warmer cloud top temperatures. On the other hand, clouds with optical thicknesses above 20 lead to larger MODIS LWP. Using cloud optical thickness as a proxy for cloud type, deep convective clouds and stratus are shown to have the poorest agreement between AMSR-E and MODIS LWP. Particularly large differences are also found at latitudes poleward of 50°. The results of this work help characterize the scene- and cloud-dependent performance of microwave and visible/near infrared retrievals of LWP.

1 Introduction

Observations of cloud liquid and ice water in the Earth's atmosphere are accompanied by poorly known uncertainties. Large differences in cloud liquid water path (LWP; see list of acronyms in the appendix) in climate models lead to large differences in predictions of the radiative influence of clouds (Houghton, 2001). Understanding the spatial and temporal variability of LWP is also relevant for the study of the hydrological and precipitation cycles (Schlosser and Houser, 2007, and references therein), and the study of aerosol indirect effects (Lohmann and Lesins, 2003; Quaas et al., 2004; Lohman and Feichter, 2005; Boers et al., 2006; Lohman et al., 2007, and references

ACPD

9, 3367–3399, 2009

therein).

All techniques for satellite-based remote sensing of clouds have limitations (Stephens and Kummerow, 2007). Even in ideal plane-parallel and optically thin stratiform clouds, many ground-based LWP observations that could be used for validation of the satellite data display significant disagreement among different measuring techniques as well (Turner et al., 2007). A better characterization of the uncertainty in LWP from different instrumental techniques is therefore crucial to our understanding of cloud processes relevant to climate variability and prediction.

Two instruments aboard the NASA Aqua spacecraft infer spatially and temporally collocated near-global, LWP fields. The Moderate Resolution Imaging Spectroradiometer (MODIS) observes visible and near-infrared radiances that are used to estimate cloud optical thickness (τ_c) and cloud effective radius (r_{eff}) (Platnick et al., 2003; King et al., 2003). MODIS liquid water path (herafter LWP_M) is then derived from these two variables after prescribing a vertical distribution of cloud water content (King et al., 2006). The Advanced Microwave Scanning Radiometer (AMSR-E) infers liquid water path (henceforth LWP_A) over water from microwave radiances at 36.5 GHz, after estimates of sea surface temperature (SST), wind speed, and column water vapor are obtained from various combinations of AMSR-E frequencies (Wentz and Meissner, 2000).

MODIS and AMSR-E sample nearly identical scenes simultaneously and hence similar LWP variability, but the different retrieval techniques and instrument sensitivities to cloud properties lead to disparities in their retrieved LWP. Near-infrared techniques are susceptible to saturation in bright clouds for τ_c values of 50–100 (Nakajima and King, 1990), and require assumptions about the vertical distribution of r_{eff} (Chang and Li, 2003; Chen et al., 2007).

Recent studies (Li et al., 2006; Boers et al., 2006; Bennartz, 2007; Horváth and Davies, 2007; Borg and Bennartz, 2007; Horváth and Gentemann, 2007; Greenwald et al., 2007) have compared satellite-based LWP derived from near-infrared, combinations of near-infrared and visible wavelengths using MODIS, and the visible frequen-

ACPD
9, 3367–3399, 2009

cies from the Multiangle Imaging Spectroradiometer (MISR), to LWP derived from microwave instruments such as AMSR-E and its predecessor, the Tropical Rainfall Measurement Mission Microwave Imager (TMI). Overviews of comparisons between passive ground-based microwave and near-infrared derived LWP to those from active measurements have also been presented in Turner et al. (2007) who described biases associated with each retrieval technique. Furthermore, Stephens and Kummerow (2007) reviewed the major sources of uncertainty in the theoretical assumptions involved in retrieving LWP with space-based instruments. These works have shown that near-infrared- and microwave-based techniques agree more closely for thin clouds with low LWP (e.g. <300 $\mathrm{g\,m^{-2}}$ in this work) and disagree for thicker clouds. Within the context of thin clouds, comparisons between microwave and near infrared satellite-based data show that the LWP differences may change sign for different types of cloud scenes. For instance, Horváth and Davies (2007) quantified biases as a function of cloud fraction and find that MODIS estimates a higher LWP than TMI for a population of overcast warm and non-precipitating clouds, but they also show that the difference changes sign with cloud fraction. In another study, Bennartz (2007) found that AMSR-E overestimates LWP relative to MODIS in overcast regions (defined as more than 0.8 cloud fraction) in the Atlantic ocean bordering South West Africa while underestimating LWP in the Atlantic off North West Africa, and in the Pacific near Northeast Asia, North, and South America for thin warm low clouds.

Other studies have shown improved agreement between MODIS and microwave-derived LWP if non-homogeneous vertical distributions of cloud liquid water are considered (Li et al., 2006; Boers et al., 2006; Chen et al., 2007; Bennartz, 2007). Such vertical distributions have been obtained either using MODIS near-infrared channels to estimate a vertical r_{eff} profile for low and warm liquid clouds (Chen et al., 2007), or using a physical parametrization to assume a vertical distribution of water and cloud droplet concentration (Boers et al., 2006; Bennartz, 2007; Borg and Bennartz, 2007). In this work, assumptions about the vertical distribution of cloud water path will be evaluated for a broad range of meteorological conditions.

ACPD
9, 3367–3399, 2009

In this study, the comparisons of LWP_M to LWP_A are stratified by additional physical cloud properties to capture a wider range of meteorological conditions than shown in previous comparisons (e.g. Horváth and Davies, 2007; Bennartz, 2007; Chen et al., 2007; Horváth and Gentemann, 2007; Borg and Bennartz, 2007). A primary objective is to asses the differences in LWP_M and LWP_A as a function of MODIS derived cloud properties: cloud fraction (CF), cloud top pressure (CTP), cloud top temperature (CTT), optical depth (τ_c), and effective radius (r_{eff}). Thus, the cloud types that are best characterized by each instrument can be identified.

This paper is arranged as follows. Section 2 discusses the comparison methodology for LWP derived from MODIS and AMSR-E and presents some illustrative global distributions of LWP_M. Section 3 presents the results of comparisons between LWP_M and LWP_A partitioned by location and the aforementioned MODIS-derived cloud physical properties. Lastly, the results of this work are discussed and summarized.

2 Data and methodology

While several retrieval versions exist for MODIS and AMSR-E, here MODIS Collection 5 and Version 5 AMSR-E (available at http://www.remss.com/, 2008) are used. The MODIS MYD06_L2 product (Platnick et al., 2003; King et al., 2006) is used to derive LWP_M, and consists of a two-channel retrieval using band 7 (2.1 µm) and either band 1 (0.66 µm), band 2 (0.86 µm), or band 5 (1.24 µm). A secondary retrieval using 1.6 µm or 2.1 µm is added in Collection 5. Retrieval quality categories are shown in Table 1 (a summary taken from King et al., 2006). The comparisons are limited to retrievals during daytime over water with marginal, good or very good confidence. As a consequence of the values shown in Table 1, we find that the selection based on the quality flags eliminates many MODIS values of $\tau_c \gtrsim 50$, and $r_{\text{eff}} \gtrsim 25$ µm, resulting in the elimination of many clouds with either very low or very high LWP values. The MODIS CF, CTT, and CTP retrievals are reported at a 5 km horizontal resolution while τ_c and r_{eff} (and therefore LWP_M) are reported at 1 km horizontal resolution. Because AMSR-E reports

ACPD
9, 3367–3399, 2009

an average LWP over 0.25°×0.25° grid cells, MODIS is averaged to the AMSR-E field of view (FOV) in the study.

Since LWP_M only exists for overcast pixels, LWP_M must be scaled by the mean CF within each AMSR-E FOV. Ice cloud sensitivity is nearly absent in AMSR-E at 37 GHz (Huang et al., 2006), whereas MODIS is highly sensitive to ice particles. To limit the comparisons to liquid clouds, only AMSR-E FOVs composed of 90% or more MODIS-defined liquid water pixels out of all cloudy pixels (ice, liquid, mixed, and undetermined phases) (Ackerman et al., 1998) are used. All cloud fractions are considered however. While MODIS reports valid LWP_M up to 10 000 g m^{-2}, Horváth and Davies (2007) show that such values are rare and, following their methodology, the comparison is restricted to LWP$\lesssim$2000 g m^{-2}.

To minimize the biases discussed above and introduced by partially filled scenes and clouds composed of ice and undetermined phase (King et al., 2006), the MODIS cloud liquid water fraction is defined as:

$$\mathrm{LWF} \equiv N_{LW}/(N_{LW} + N_{IW} + N_{UW}) \quad (1)$$

where N_{LW} is the frequency of cloud liquid water within an AMSR-E FOV, and likewise N_{IW} and N_{UW} are the frequencies of ice and undetermined cloud phase, respectively. The cloud liquid fraction (CLF) ratio was then calculated by the following:

$$\mathrm{CLF} \equiv \mathrm{CF} \times \mathrm{LWF}. \quad (2)$$

Therefore, we can define MODIS LWP_M as:

$$LWP_M \equiv \mathrm{CLF} \times CWP_M \quad (3)$$

where CWP_M indicates the total cloud water path of MODIS (liquid+ice+undetermined) within an AMSR-E FOV.

This study is limited to 16 days because of the size of the MODIS data sets. To minimize the influence of seasonal biases, the equinoxes and solstices were selected during the years 2003–2006. This study considers all clouds equatorward of 85° latitude over a large range of CF, CTP, CTT, solar zenith angles, and precipitation states

ACPD
9, 3367–3399, 2009

for LWF>0.9. As discussed in the introduction, previous studies have focused on more limited conditions. Li et al. (2006) considered only warm water clouds (CTT>273°K) during January 2003 between 40° N and 40° S. Horváth and Davies (2007) analyzed 400 random orbits mostly within April 2001, July–August 2003, and February 2004 with solar zenith angles limited between 17° and 53°, while partitioning statistics of precipitating and non-precipitating clouds with TMI-derived rainfall. As in this work, Li et al. (2006) and Horváth and Davies (2007) used 0.25°×0.25° grids for the comparison standard. Two additional studies used 1°×1° spatial resolution and a longer time span: Bennartz (2007) investigated five regions equatorward of 45° latitude from July 2002–December 2004; Borg and Bennartz (2007) used MODIS level 3 data from 2004 and selected CTT>263°K, LWF>0.98 and a solar zenith angle <70°.

Figure 1 shows the global mean maps of CWP_M and LWF over the 8 equinox days. Figure 1a shows that low latitudes contain more regions with smaller CWP_M than at higher latitudes. Figure 1b shows that LWF is smallest above elevated topographic features such as mountain ranges, and also at high latitudes. Over the oceans, where the comparisons below are carried out, there are several distinctive areas of high LWF near the western coasts of S. and N. America, Africa, and Australia associated with stratocumulus layers under regions of strong subsidence. As shown below, these areas are found to typically have LWP_M>LWP_A.

The nominal error for MODIS τ_c is estimated to be close to 10% for individual retrievals with a relative random component of 20% (Horváth and Davies, 2007). Table 2 shows the mean differences that are found in the present study between the primary and secondary MODIS retrievals, and are partitioned into "thin" and "thick" clouds. The difference for thin clouds is consistent with the MODIS error estimates while it is slightly larger for thicker clouds. When all cloud types are considered, the median is within $10\,g\,m^{-2}$, which is the precission in the reported AMSR-E LWP_A product. As a result, the bias introduced by comparing AMSR-E to either one of the two MODIS LWP retrievals is smaller than the AMSR-E reported uncertainty and the distinction between the two is not considered further in this work.

ACPD
9, 3367–3399, 2009

Given the agreement between the primary and secondary LWP_M, an average of both MODIS retrievals was used ($CLWP_M$). When MODIS reports only one of the two retrievals that value is used; otherwise, the average of the primary and the secondary retrieval is used. This approach increases the number of matched differences to AMSR-E, with a minimal risk of introducing significant biases in the MODIS signal.

3 LWP differences as a function of cloud properties

The differences between the MODIS primary (combined) minus AMSR-E LWP $\equiv\Delta$LWP(ΔCLWP) are summarized in Table 3. To facilitate the comparison to previous studies, the results are also partitioned into categories of thin clouds (LWP<300 g m^{-2}) as well as broken (CF$\leq$0.8) or overcast (CF>0.8) clouds.

In Sect. 2, Eqs. (1–3) provide the means to "correct" for cloud heterogeneity and the ice phase determined by MODIS within the AMSR-E FOV. Cloud heterogeneity and instrument sensitivity to cloud phase were tested and a noticeable decrease in ΔLWP occurs when these effects are accounted for (leftmost column vs. all other columns in Table 3). When screening for ice phase clouds and correcting by cloud fraction, the mean ΔLWP decreases from 45.8 g m^{-2} to 25.7 g m^{-2} (not shown in Table 3). For LWF>0.9, ΔLWP decreases further to a mean of 14.3 g m^{-2} (second column in Table 3). Similar decreases in the standard deviation of ΔLWP for increasing LWF are also observed. After correcting for cloud heterogeneity, the poorest agreement is found for scenes with all (thin and thick) clouds (ΔLWP=17.9 g m^{-2}) over the sixteen days considered in this study. The conditions that show the smallest mean difference are for a combination of primary and secondary LWP_M within thin, broken and overcast scenes (ΔCLWP=11.2 g m^{-2}).

Wentz (1997) estimates that uncertainties due to random error for individual retrievals of LWP_A are approximately 25 g m^{-2}, where about 20% of the error is caused by radiometric noise. A more recent description of error sources and error propagation in AMSR-E LWP retrievals (O'Dell et al., 2008) is consistent with this value. In Table 3,

the median and mean ΔLWP are within this uncertainty, although the standard deviations are approximately twice this value. Given the large sample size considered in this work, the mean and median differences cannot be explained by random error either in MODIS or AMSR-E retrievals but rather are indicative of systematic biases in one or both data sets that depend on the observed cloud conditions.

Figure 2 presents histograms of ΔLWP and ΔCLWP for all clouds as well as for thin clouds only (defined by a threshold of 300 g m^{-2}). Note that the mode and median in Table 3 are slightly smaller than the mean, indicating a positive skewness. The skewness and ΔCLWP increase significantly when the MODIS cloud phase is ignored (broken red line in Fig. 2b). Additionally, the smallest bias and skewness exist for LWF>0.9 (yellow in Fig. 2a and thin black in Fig. 2b) where the combined MODIS CLWP$_M$ is used.

3.1 Cloud water vertical distributions

Figure 3 shows a 2-D probability distribution function (PDF) of CLWP$_M$ vs. LWP$_A$ for a subset of thin clouds (LWP<300 g m^{-2}). For the smallest values of LWP, CLWP$_M$ is on average smaller than LWP$_A$, while the opposite is true for higher LWP. Previous studies have shown that the assumed vertical distribution of liquid water affects the relationship between LWP, τ_c and r_{eff} (Boers et al., 2006; Bennartz, 2007; Chang and Li, 2003; Stephens and Kummerow, 2007, and references therein). Therefore, two different vertical cloud water distributions (e.g. Bennartz, 2007) are considered in Fig. 3:

$$\text{Vertically uniform clouds}: \quad \text{LWP}_M = \frac{4\rho_i}{3Q_e(r_{\text{eff}})}\tau_c r_{\text{eff}} \tag{4}$$

and

$$\text{Stratified clouds}: \quad \text{LWP}_M = \frac{10\rho_i}{9Q_e(r_{\text{eff}})}\tau_c r_{\text{eff}}. \tag{5}$$

Equation (4) assumes a vertically constant number of cloud droplets and is used in the MODIS standard retrievals, while Eq. (5) corresponds to an adiabatic distribution

of r_{eff} with height. It is obtained simply by scaling Eq. (4) by 5/6. The two vertical stratifications are marked in Fig. 3 by the black (Eq. 4) and green line (Eq. 5). At lower LWP, the mean differences are in better agreement with a uniform vertical distribution of LWP as in Eq. (4), but both vertical distributions are barely discernible from each other. However, as LWP increases, the mean differences are in better agreement with the stratified LWP (Eq. 5). This result is nearly identical for overcast scenes of CF>0.8 or when using only the primary LWP_M retrieval.

Figure 4 shows the mean ΔCLWP as a function of $CLWP_M$ for thin clouds. It provides further evidence that a pseudoadiabatic LWP profile may be a better approximation for the calculation of LWP_M at values of LWP>40 g m^{-2}. Figure 4 clearly shows that MODIS is lower (higher) than AMSR-E below (at or above) 40 g m^{-2}. The magnitude of ΔLWP is within the single FOV retrieval uncertainty of AMSR-E below 120 g m^{-2} for the uniform assumption of Eq. (4). However, in the case of assuming a stratified cloud water distribution, the magnitude of ΔLWP is within the single AMSR-E retrieval uncertainty for $CLWP_M$ below 240 g m^{-2}. These results are similar for regions with CF>0.8 (not shown).

Recent studies that have addressed ΔLWP in the thinnest clouds (including the present study) have found that MW-derived cloud liquid water is greater than that derived from VIS-NIR radiances. Horváth and Davies (2007) also showed this is the case between TMI and MODIS. However, measurement sensitivity to LWP alone cannot explain the sign changes in ΔCLWP between different geographical locations as reported by Bennartz (2007). This behaviour will be addressed further in the following sub-sections.

3.2 Cloud fraction and cloud top pressure

The earlier comparisons presented in Table 3 provide insights into the influence of CF on ΔLWP. The agreement is tighter for comparisons limited to thin clouds (LWP<300 g m^{-2}), with a mean difference and one standard deviation of 14.7±39.8 g m^{-2}. This improves slightly to 11.2±39.3 g m^{-2} when one uses the com-

bined MODIS LWP and calculates $\Delta CLWP_M$.

Horváth and Davies (2007) reported differences of TMI and MODIS $\Delta LWP = 4\,g\,m^{-2}$ in warm non-precipitating thin clouds and $-5\,g\,m^{-2}$ for overcast warm non-precipitating clouds. The biases presented here between AMSR-E and MODIS Collection 5 exceed those reported by Horváth and Davies (2007). A possible explanation for the larger biases in our study is the ellimination of certain atmospheric conditions from their study. For instance, after using TMI to consider only non-precipitating clouds, Horváth and Davies (2007) found that most of their warm, liquid, and non-precipitating clouds with less than $300\,g\,m^{-2}$ are boundary layer clouds with CTP>700 hPa (called by them "BL1", and "BL2" for overcast scenes). Furthermore, they associated clouds with $LWP_M > 300\,g\,m^{-2}$ to deep convective liquid clouds. Figure 5 shows that the thin clouds studied here span over a wider range of pressures than that of Horváth and Davies (2007).

The main difference between BL1 and BL2 in Horváth and Davies (2007) was the magnitude of CF. This motivated the stratification of ΔLWP into 0.1-wide CF intervals, and they showed that the largest negative ΔLWP occurred for small CF. As CF increased, negative values of ΔLWP gradually switched to positive at CF>0.65. Three explanations were given for the ΔLWP dependence on CF: 1) the absorption model used in the MW retrieval algorithms; 2) the truncation of the MW data set at $LWP = 0\,g\,m^{-2}$, and; 3) the MODIS cloud mask may have missed a significant number of shallow cumulus clouds, causing an underestimation in the subdomain CF and domain-averaged LWP_M. Additionally, the process of averaging to $0.25^\circ \times 0.25^\circ$ before multiplying LWP by the averaged CF in each bin, results in smaller LWP_M than if the product is done at 5 km resolution before averaging and this contributes to the negative ΔLWP. This error source does not have a simple correction because one needs CF and LWP_M at the same spatial resolution.

Figure 5 shows ΔCLWP as a function of CF and CTP and it illustrates that the changes in sign and magnitude vary with both CF and CTP. At CF<0.4, ΔCLWP is negative for all clouds. However, for CF>0.4 ΔCLWP can be positive, near zero or

ACPD
9, 3367–3399, 2009

negative for high clouds (lower CTP). These results show that LWP_M is biased low relative to LWP_A, not only in broken cloud scenes with CF<0.4, but also in higher clouds with CF>0.7.

Thicker clouds (LWP>300 g m^{-2}) show similar tendencies as the thin clouds presented in Fig. 5. In thicker clouds, ΔCLWP is even larger than in thinner clouds. Furthermore, the sign change occurs for CF=0.6–0.7 and CTP=750–850 hPa (not shown).

In summary, the cloud population used in this work shows negative ΔCLWP across all cloud types with CF<0.4 and for CF between 0.4–0.9, LWP_A>LWP_M in scenes dominated by the higher cloud tops (lower CTP). The CF-related biases are in general agreement with Horváth and Davies (2007) and Horváth and Gentemann (2007), but these results demonstrate that the biases of ΔCLWP depend on both CF and CTP (i.e. cloud top height) in a complex manner.

3.3 Cloud geographical distribution

In an analysis of ΔLWP in six overcast regions containing maritime boundary layer clouds, Bennartz (2007) showed that, an adiabatic stratification assumption (Eq. 5) gives a positive ΔLWP in the South Eastern Pacific, West of South America, and North West Pacific off Asia, West of North America and West of North Africa. In contrast, the sign of ΔLWP changes in the South Eastern Atlantic ocean bordering Namibia. The sign change is explained by Bennartz (2007) as possible contamination of vertical layering of smoke from biomass burning on top of liquid water clouds as observed by MODIS. That work shows that ΔLWP may change sign with location. To compare with the results of Bennartz (2007), Fig. 6a shows the geographical distribution of ΔCLWP for thin and overcast clouds, while Fig. 6b shows the frequency of ΔCLWP by latitude. In general, $CLWP_M$>LWP_A for thin and overcast clouds in high latitudes, while the reverse may be true for low latitude regions containing deep convective clouds.

In summary, Fig. 6b shows a latitude dependence of ΔCLWP; however, there are important zonal asymmetries as suggested by Fig. 6a. AMSR-E tends to overestimate LWP (relative to MODIS) at tropical and some subtropical latitudes, but tends to un-

ACPD
9, 3367–3399, 2009

derestimate LWP over the eastern boundary currents at the subtropical and tropical latitudes off of North and South America and South Africa. The northern boundary current bordering subtropical North Africa is an exception to the overestimation in regions dominated by stratocumulus pointed out by Bennartz (2007). The latitude and regional dependence of ΔCLWP suggests quantifying the differences by cloud-type variations. As a proxy for cloud type, the dependence of ΔCLWP biases on τ_c, r_{eff}, and CTT is described in the following subsections.

3.4 τ_c and r_{eff}

Figure 7 shows ΔCLWP for thin clouds as a function of the CLWP_M and τ_c. Clouds with $\tau_c<5$ have mean $\text{LWP}_A>\text{CLWP}_M$. For thin clouds ($\text{LWP}<300\,\text{g}\,\text{m}^{-2}$), both instruments show agreement to within $25\,\text{g}\,\text{m}^{-2}$ (approximate uncertainties of CLWP_M and LWP_A) for $\text{CLWP}_M<120\,\text{g}\,\text{m}^{-2}$ and $5<\tau_c<30$. ΔCLWP increases more substantially when transitioning to more opaque clouds. Furthermore, ΔCLWP decreases when cases are limited to overcast scenes only (Fig. 7b).

Note that the best agreement between LWP_A and CLWP_M is found for clouds with $\tau_c<20$, which are classified by the International Satellite Cloud Climatology Project (ISCCP; Rossow and Schiffer, 1999) as cirrostratus, altostratus and stratocumulus, depending on their altitude. The more opaque clouds ($20<\tau_c<40$) like ISCCP-defined cumulonimbus, nimbostratus and stratus reveal poorer agreement. This suggests systematic instrumental differences and sampling biases for entire classes of clouds, and their associated physical processes.

Figure 8 shows ΔCLWP as a function of τ_c and r_{eff} within overcast scenes. Here, AMSR-E overestimates higher LWP than MODIS for clouds with the smallest τ_c independently of r_{eff}. Clouds with higher τ_c (>20) show larger discrepancies of LWP that are a function of r_{eff}. Comparing to Fig. 7a, ΔCLWP is highest for optically thin clouds ($\tau_c<20$) with the largest values of CLWP_M. Furthermore, for optical thicknesses of 20–40, the increase in ΔCLWP is most pronounced for larger values of r_{eff}, but for

ACPD
9, 3367–3399, 2009

$r_{\text{eff}} \leq 10\,\mu\text{m}$ and $\tau_c < 20$, ΔCLWP is within the stated uncertainties of MODIS and AMSR-E derived LWP. This dependence of ΔCLWP on r_{eff} is generally consistent with larger r_{eff} being attributed more frequently to precipitating clouds (Chen et al., 2007) which are included in this study.

3.5 Cloud top temperature

For the same data presented in the previous sections, Fig. 9 shows CLWP_M, ΔCLWP, r_{eff}, and τ_c as a function of both CTT and CTP. Figure 9a shows the mean CLWP_M as a function of CTP and CTT. For Fig. 9a at a given CTP, MODIS shows that warmer cloud tops have lower CLWP_M, except for CTP~300–600 hPa. A few clouds have CTT<233 K, even though we are only considering cloud regions with 90% or more cloud water reported as liquid. An initial exploration of a MODIS granule on 23 September 2006 (S. L. Nasiri, personal communication, 2008) and comparison to coincident CLOUDSAT and CALIPSO profiles showed that cirrus contamination may be the root cause leading an inexact retrieval of CTT that assigned an equally low CTT to a cirrus sub-region and to lower possibly warmer clouds. The other possible explanation that was explored is a missclassification of MODIS cloud phase. MODIS cloud phase is inferred with a shortwave IR reflectance ratio threshold that depends on the underlying surface type. These phase tests are applied only when clouds are thick enough to cause appreciable liquid/ice shortwave IR absorption. In the granule analyzed MODIS cloud phase seemed to correctly identify ice in the cirrus region and water in the lower clouds. Figure 9a shows that cold cloud tops, as well as low and warm clouds, are characterized by very low CLWP_M. The highest CLWP_M are found between 400–900 hPa and 240–280 K. The peak CLWP_M is observed for cold clouds (CTT<260 K) and between 600–900 hPa.

Figure 9b shows that ΔCLWP at a fixed CTP is a strong function of CTT; ΔCLWP can even change sign as highlighted by the thick black zero-contour line. In general, $\text{CLWP}_M > \text{LWP}_A$ for low CTT, and $\text{LWP}_A > \text{CLWP}_M$ for high CTT. The largest positive ΔCLWP is found at CTP 900–600 hPa and CTT<260 K.

ACPD
9, 3367–3399, 2009

The average r_{eff} is shown as a function of CTT and CTP in Fig. 9c, and shows a tendency for larger r_{eff} to correspond to $\text{LWP}_A > \text{CLWP}_M$ when CTT>240 K. Also, the highest and coldest cloud tops (CTP<400 hPa and CTT<240 K) coincide with clouds having the largest average r_{eff}. The large ΔCLWP in Fig. 9b is not mirrored by any particular patterns in r_{eff} observed in Fig. 9c, but is reflected in the high values of τ_c (Fig. 9d). Further discussion of this feature is presented in the following subsection.

The results presented here may reconcile apparently contradictory conclusions from earlier studies. Selected bounds of CTT and CTP will ultimately influence conclusions drawn about ΔLWP. Borg and Bennartz (2007) limited their comparisons to warm clouds with CTT>268 K and CF>0.98, while Li et al. (2006) limited the comparison to CTT>273 K and high CTP. Results shown here are consistent with the ΔLWP reported in those works.

3.6 Locations of anomalies

Figure 10 shows the spatial distributions of the ΔLWP anomalies discussed in the previous subsection. Figure 10a shows the relative frequency of ΔCLWP<0 for clouds with CTP>250 hPa. For the sample data set used here, AMSR-E reports higher LWP on more days (blue colors) at low latitudes while MODIS reports higher LWP (brown colors) at mid-to high latitudes. Overall MODIS tends to report higher LWP than AMSR-E everywhere except for a small portion of the tropics and subtropics. Figure 10b maps the occurrence of large ΔCLWP in 9b (CTP>700 hPa, CTT<260 K). These opaque, low and cold clouds responsible for the largest positive CLWP_M and ΔCLWP are generally found poleward of 50°. The cause of this large difference needs further study, but could be associated with the misassignment of cloud phase by MODIS (Nasiri and Kahn, 2008).

ACPD
9, 3367–3399, 2009

4 Summary and conclusions

Satellite-derived cloud liquid water path (LWP) from the Moderate Resolution Imaging Spectroradiometer (MODIS) and the Advanced Microwave Scanning Radiometer (AMSR-E) are compared and stratified by cloud physical properties retrieved from MODIS. The comparison uses both MODIS primary and secondary LWP retrievals independent of the occurrence of precipitation. Two types of vertical cloud water distributions that are frequently used are tested on the MODIS retrievals: vertically uniform and stratified cloud water distributions.

In general, MODIS liquid water path retrievals (LWP_M) are most similar to AMSR-E LWP_A in moderately overcast scenes (Fig. 5). If the differences of LWP (ΔLWP) are considered as a function of the magnitude of LWP, then $LWP_A > LWP_M$ for small LWP ($<40\,g\,m^{-2}$). The smallest differences in ΔLWP are generally found for $LWP < 130\,g\,m^{-2}$ assuming vertically uniform cloud water (Fig. 4) and $LWP < 240\,g\,m^{-2}$ for vertically stratified cloud water distributions as discussed in (Boers et al., 2006; Bennartz, 2007; Borg and Bennartz, 2007). This suggests that observed cloud water vertical structures are frequently vertically stratified.

Furthermore, the differences of ΔLWP between visible/near infrared and microwave retrievals vary with cloud fraction (CF), cloud top temperature (CTT) and pressure (CTP). Larger values of CF often correlate to values of $LWP_A < LWP_M$, consistent with findings of previous studies (Horváth and Davies, 2007; Horváth and Gentemann, 2007). On the contrary, when low and broken clouds are considered, LWP_M is frequently less than LWP_A (Fig. 5).

When discriminating values of ΔLWP by τ_c, the magnitude is larger than the nominal instrument uncertainties of both AMSR-E and MODIS for optically thick cloud types: cumulonimbus, nimbostratus and stratus using the cloud typing methodology of the International Satellite Cloud Climatology Project (ISCCP; Rossow and Schiffer, 1999). Warmer cloud tops are associated with larger LWP_A and relatively smaller r_{eff}. Conversely, colder cloud tops are associated with smaller LWP_A. This behaviour is con-

ACPD
9, 3367–3399, 2009

sistent with the direction of changes associated to errors in LWP_A retrievals as a a consequence of improper CTT estimates (O'Dell et al., 2008). Geographical distributions of ΔCLWP (Fig. 6) demonstrate that at low latitudes, LWP_A is generally larger than $CLWP_M$ but the reverse is true for regions near or over the eastern boundary currents dominated by stratocumulus.

The results of this study are largely consistent with previous LWP intercomparison studies, but also suggest possible reasons for the aspects of disagreement among them; namely, that limited ranges of atmospheric conditions and cloud types can yield different values of ΔLWP. Horváth and Davies (2007, and references therein) show that MODIS LWP are larger than AMSR-E on a global basis but are a function of CF. Bennartz (2007) and Borg and Bennartz (2007) find that ΔLWP can change sign between different regions. These works did not consider the coldest and thinnest (lowest LWP) clouds that are included in this study. Different locations are dominated by different meteorological conditions, cloud types, and cloud properties, which correlate with the magnitude of ΔLWP.

This study demonstrates the utility of multi-sensor derived LWP and quantifies the instrument differences with cloud varying properties derived from MODIS. Furthermore, this work is expected to help quantify the sampling strengths and limitations of visible/near infrared and microwave imagers to assess global cloud distributions.

Acknowledgements. Conversations with S. Platnick and S. Nasiri are gratefully acknowledged. Funding for this work has been provided by NASA through the NASA Energy and Water cycle Studies (NEWS) program. BHK was supported by the NASA Post-doctoral program during this study. The research described in this Paper was carried out at the Jet Propulsion Laboratory/California Institute of Technology, under a contract with the National Aeronautics and Space Administration.

Appendix A

List of symbols and acronyms

Symbol or Acronym	Meaning
CF	MODIS cloud fraction
CLF	MODIS liquid cloud fraction
$CLWP_M$	MODIS liquid water path combining standard and secondary LWP retrievals
CTP	MODIS cloud top pressure
CTT	MODIS Cloud top temperature
CWP_M	MODIS cloud water path (all phases)
$\Delta CLWP$	$CLWP_M - LWP_A$
ΔLWP	$LWP_M - LWP_A$
LWF	Liquid water ratio of the combined primary MODIS retrievals
LWP	Liquid Water Path
LWP_A	AMSR-E liquid water path
LWP_M	MODIS liquid water path
PDF	Probability Distribution Function
r_{eff}	MODIS cloud effective radius (CER)
SST	Sea Surface Temperature
τ_c	MODIS cloud optical thickness (COT)

References

Ackerman, S. A., Strabaja, K. I., Menzel, W., Frey, R., Moeller, C., and Gumley, L.: Discriminating clear sky from clouds with MODIS, J. Geophys. Res., 103, 32141–32157, 1998. 3372

Bennartz, R.: Global assessment of marine boundary layer cloud droplet number concentration

from satellite, J. Geophys. Res., 112, D02201, doi:10.1029/2006JD007547, 2007. 3369, 3370, 3371, 3373, 3375, 3376, 3378, 3379, 3382, 3383

Boers, R., Acarreta, J. R., and Gras, J. L.: Satellite monitoring of the first indirect aerosol effect: Retrieval of the droplet concentration of water clouds, J. Geophys. Res., 111, D22208, doi:10.1029/2005JD006838, 2006. 3368, 3369, 3370, 3375, 3382

Borg, L. A. and Bennartz, R.: Vertical structure of stratiform marine boundary layer clouds and its impact on cloud albedo, Geophys. Res. Lett., 34, L05807, doi:10.1029/2006GL028713, 2007. 3369, 3370, 3371, 3373, 3381, 3382, 3383

Chang, F.-L. and Li, Z.: Retrieving vertical profiles of water-cloud droplet effective radius: Algorithm modification and preliminary application, J. Geophys. Res., 108, 4763–4772, 2003. 3369, 3375

Chen, R., Chang, F.-L., Li, Z., Ferraro, R., and Weng, F.: Impact of the vertical variation of cloud droplet size on the estimation of cloud liquid water path and rain detection, J. Atmos. Sci., 64, 3843–3853, 2007. 3369, 3370, 3371, 3380

Greenwald, T. J., L'Ecuyer, T. S., and Christopher, S. A.: Evaluating specific error characteristics of microwave-derived cloud liquid water products, Geophys. Res. Lett., 34, L22907, doi:10.1029/2007GL031180, 2007. 3369

Horváth, A. and Davies, R.: Comparison of microwave and optical cloud water path estimates from TMI, MODIS and MISR, J. Geophys. Res. Atmos., 112, D01201, doi:10.1029/2006JD007101, 2007. 3369, 3370, 3371, 3372, 3373, 3376, 3377, 3378, 3382, 3383

Horváth, A. and Gentemann, C.: Cloud-fraction-dependent bias in satellite liquid water path retrievals of shallow, non-precipitating marine clouds, Geophys. Res. Lett., 34, L22806, doi:10.1029/2007GL030625, 2007. 3369, 3371, 3378, 3382

Huang, J., Minnis, P., Lin, B., Yi, Y., Fan, T.-F., Sun-Mack, S., and Ayers, J.: Determination of ice water path in ice-over-water cloud systems using combined MODIS and AMSR-E measurements, Geophys. Res. Lett., 33, L21801, doi:10.1029/2006GL027038, 2006. 3372

King, M. D., Platnick, S., Hubanks, P. A., Arnold, G. T., Moody, E. G., Wind, G., and Wind, B.: Collection 005 Change Summary for the MODIS Cloud Optical Property (06_OD) Algorithm, available at http://modis-atmos.gsfc.nasa.gov/products_C005update.html, 2006. 3371, 3372

Li, Z., Chen, R., and Chang, F.-L.: The Impact of the Vertical Variation of Cloud Droplet Size on the Estimation of Cloud Liquid Water Path and Its Potential for Rain Detection, in: Sixteenth Arm Science Team Meeting Proceedings, 2006. 3369, 3370, 3373, 3381

Lohmann, U. and Feichter, J.: Global indirect aerosol effects: a review, Atmos. Chem. Phys., 5, 715–737, 2005, http://www.atmos-chem-phys.net/5/715/2005/. 3368
Lohman, U., Quaas, J., Kinne, S., and Feichter, J.: Different Approaches for Constraining Global Climate Models of the Anthropogenic Indirect Aerosol Effect, B. Am. Meteorol. Soc., pp. 243–250, 2007. 3368
Lohmann, U. and Lesins, G.: Comparing continental and oceanic cloud susceptibilities to aerosols, Geophys. Res. Lett., 30, 1791, doi:10.1029/2003GL017828, 2003. 3368
Nakajima, T. and King, M.: Determination of the optical thickness and effective particle radius of clouds from reflected solar radiation measurements. Part I: Theory, J. Atmos. Sci., 47, 1878–1893, 1990. 3369
Nasiri, S. and Kahn, B. H.: Limitations of bispectral infrared cloud phase determination and-potential for improvement, J. Appl. Meteor., 47, 2895–2910, doi:10.1175/2008JAMC1879.1, 2008. 3381
O'Dell, C. W., Wentz, F. J., and Bennartz, R.: Cloud liquid water path from satellite-based passive microwave observations: a new climatology over the global oceans, J. Climate, 21, 1721–1739, 2008. 3374, 3383
Platnick, S., King, M., Ackerman, S., Menzel, W., Baum, B., Riedl, C., and Frey, R.: The MODIS cloud products: algorithms and examples from Terra, IEEE Trans. Geosci. Rem. Sens., Aqua Special Issue, 41, 459–473, 2003. 3371
Quaas, J., Boucher, O., and Breon, F.-M.: Aerosol indirect effects in POLDER satellite data and the Laboratoire de Meteorologie Dynamique-Zoom (LMDZ) general circulation model, J. Geophys. Res., 109, D08205, doi:10.1029/2003JD004, 2004. 3368
Rossow, W. B. and Schiffer, R. A.: Advances in understanding clouds from ISCCP, B. Am. Meteorol. Soc., 80, 2261–2287, 1999. 3379, 3382
Schlosser, C. A. and Houser, P. R.: Assessing a Satellite-Era Perspective of the Global Water Cycle, J. Climate, 20, 1316–1338, doi:10.1175/JCLI4057.1, 2007. 3368
Stephens, G. L. and Kummerow, C.: The remote sensing of clouds and precipitation from space: A review, J. Atmos. Sci., 64, 3742–3765, 2007. 3369, 3375
Wentz, F. J.: A well-calibrated ocean algorithm for special sensor microwave/imager, J. Geophys. Res., 102, 8703–8718, 1997. 3374
Wentz, F. J. and Meissner, T.: Algorithm Theoretical Basis Document (ATBD). Version 2. AMSR Ocean Algorithm, Tech. Rep. RSS Tech. Proposal 121599 A-1, Remote Sensing Systems, 2000. 3369

Table 1. Confidence flag assignment criteria for liquid water clouds. This study is limited to marginal, good and very good quality over ocean during daytime.

τ_c	r_{eff}			
	2–4 µm	4–20 µm	20–25 µm	25–30 µm
0–2	No Confidence	Good	Marginal	No Confidence
2–100	Marginal	Very Good	Good	Marginal

Table 2. Differences between MODIS primary and MODIS 1.6 µm and 2.1 µm retrievals.

$CLWP_M$	Mean	Median	Mode	Std. Dev.
$<300\,g\,m^{-2}$	−5.3	5	3.3	109.5
$>300\,g\,m^{-2}$	48.3	95	138.5	435.1

ACPD
9, 3367–3399, 2009

Table 3. Comparisons between MODIS and AMSR-E LWP under different conditions. Double lines separate the primary MODIS retrieval and combined primary and secondary (1.6/2.1 µm) retrievals for each bin average of LWP_M. The differences for overcast cloud liquid fraction scenes (CF>0.8) is given in a separate column. The differences for thin LWP is also shown. Bold values highlight the scenarios with the best agreement.Thin clouds are defined as those with LWP_M and LWP_A<300 g m^{-2}.

	Primary ΔLWP				Combined ΔCLWP		
	All CF All clouds All phases	All CF All clouds	CF>0.8 All clouds	CF>0.8 Thin clouds	All CF Thin clouds	All CF All clouds	CF>0.8 Thin clouds
				Liquid phase (LWF>0.9) CLF Corrected			
N	5 106 697	2 663 543	1 832 779	1 752 816	2 562 246	2 672 779	1 740 050
Mean	45.8	14.3	17.9	14.7	**11.2**	15.2	15.6
Median	15.9	6.5	10.5	9.9	**5.4**	6.2	9.9
Mode	7.7	2.8	6.6	6.7	1.8	**1.2**	5.9
Std. Dev.	127.3	52.7	56.1	39.8	**39.3**	55.1	42.2

ACPD
9, 3367–3399, 2009

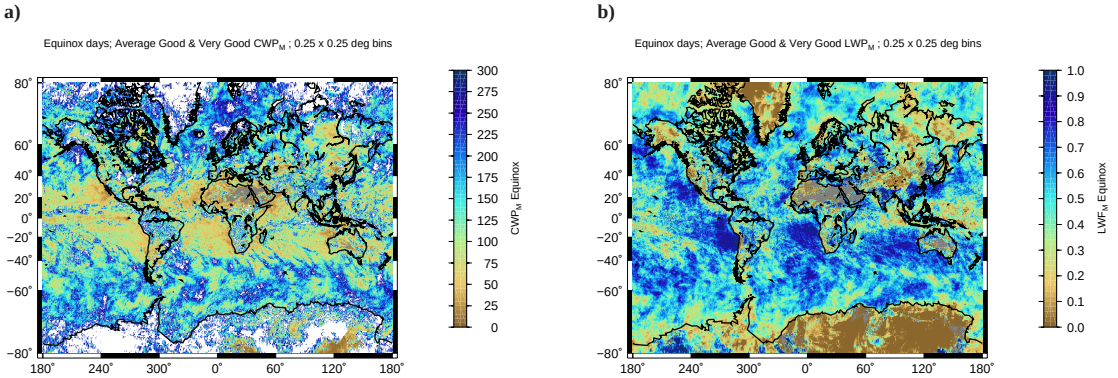

Fig. 1. Climatology of **(a)** CWP_M, and **(b)** LWF averaged over all equinox days during 2003–2006.

ACPD
9, 3367–3399, 2009

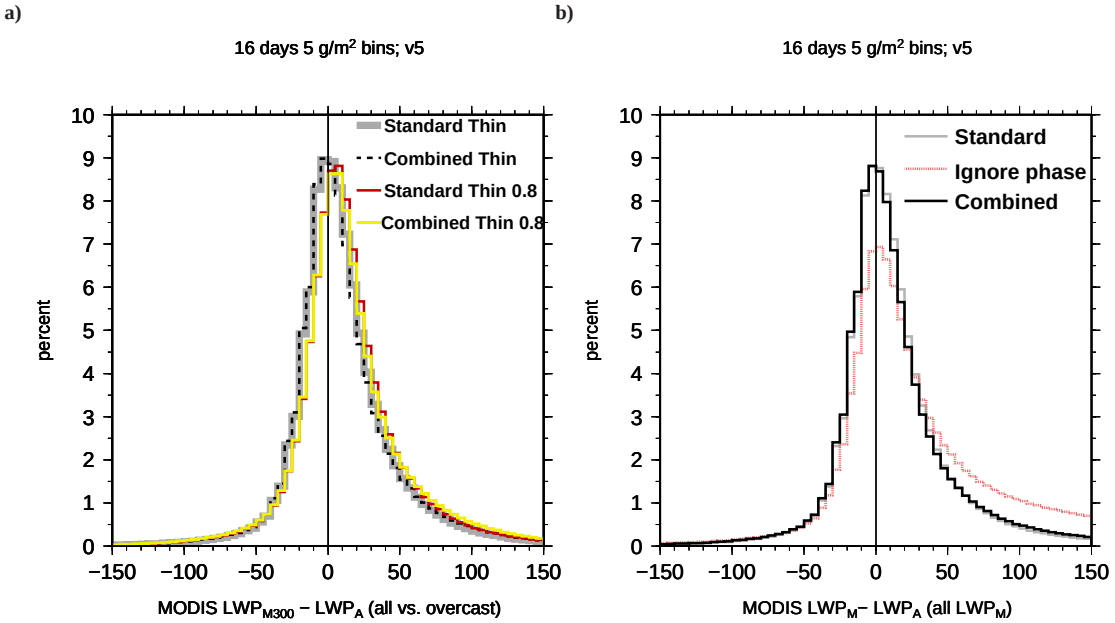

Fig. 2. **(a)** Differences between LWP_M and LWP_A for thin clouds in bins of $5\,g\,m^{-2}$. Thick grey line is for thin liquid clouds and all cloud fractions for LWF>0.9; thin black dashed line for combined primary and secondary MODIS retrievals of the same conditions; red line is for thin liquid clouds in overcast bins with CF>0.8 and LWF>0.9; thin yellow line is for combined primary and secondary MODIS retrievals of the same scenes as the red line. **(b)** Differences between LWP_M and LWP_A for all clouds when LWF>0.9. The grey line marks all liquid cloud values of CF; the red line is when the cloud phase is ignored (liquid or not) using a combination of primary and secondary MODIS retrievals; thin black line for liquid clouds combining primary and secondary MODIS retrievals where LWF>0.9.

ACPD
9, 3367–3399, 2009

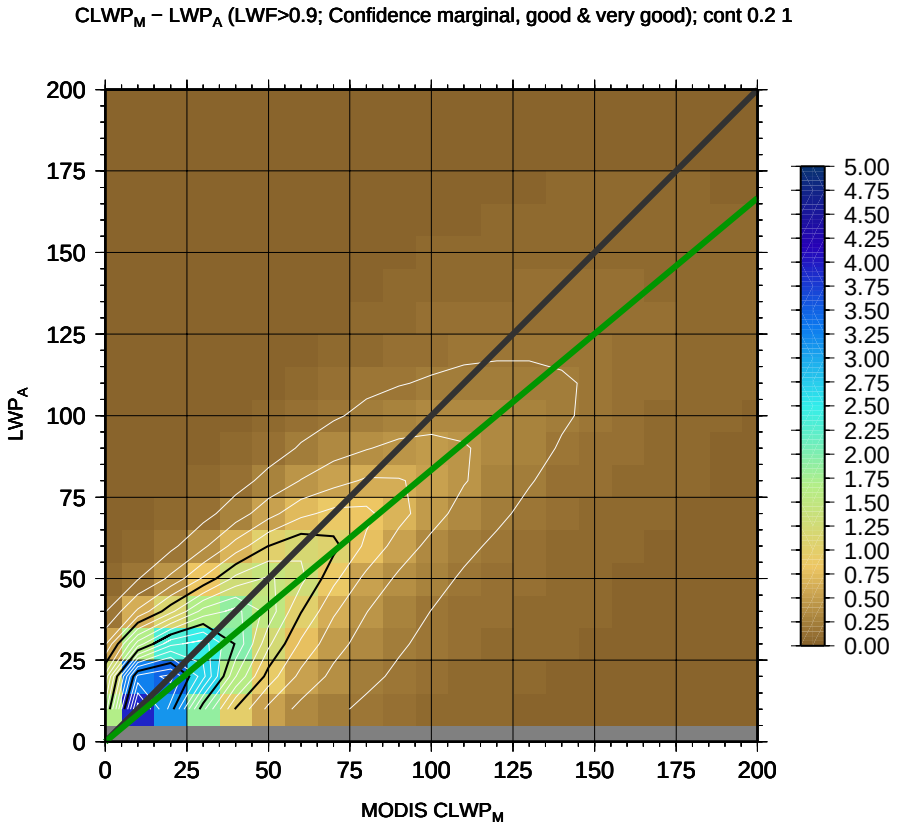

Fig. 3. Two-dimensional PDF of CLWP$_M$ vs. LWP$_A$ for thin clouds. Contour lines mark the frequency of a given combination of LWP$_A$ and CLWP$_M$. Light contour lines are 0.2% increments while dark contour lines mark 1% increments. The thick black line shows the difference expected if the vertical distribution of cloud water content is homogeneous following Eq. (4), while the green line marks the expected mean difference for vertical stratification of cloud water content following Eq. (5).

ACPD
9, 3367–3399, 2009

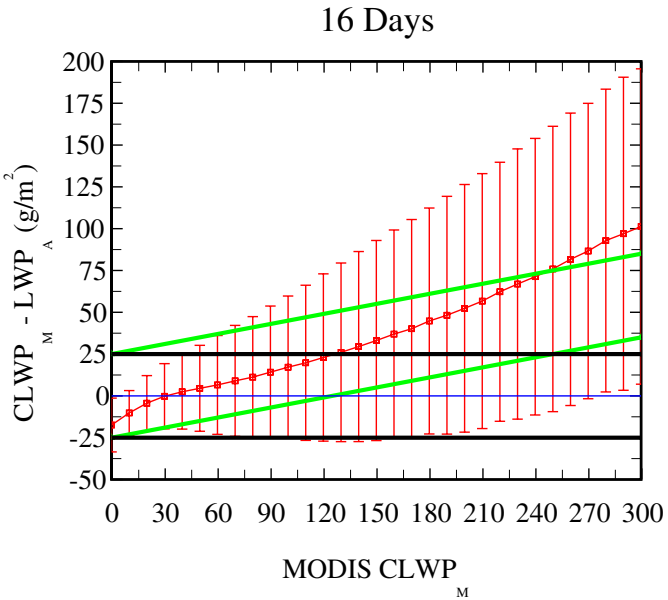

Fig. 4. ΔCLWP vs. $CLWP_M$ for thin clouds (red line) over 16 days distributed in 2003 to 2006. The vertical bars are twice the standard deviation. The parallel black solid lines show 25 g m^{-2} errors assuming a homogeneous cloud liquid water distribution, and green for vertically stratified.

ACPD
9, 3367–3399, 2009

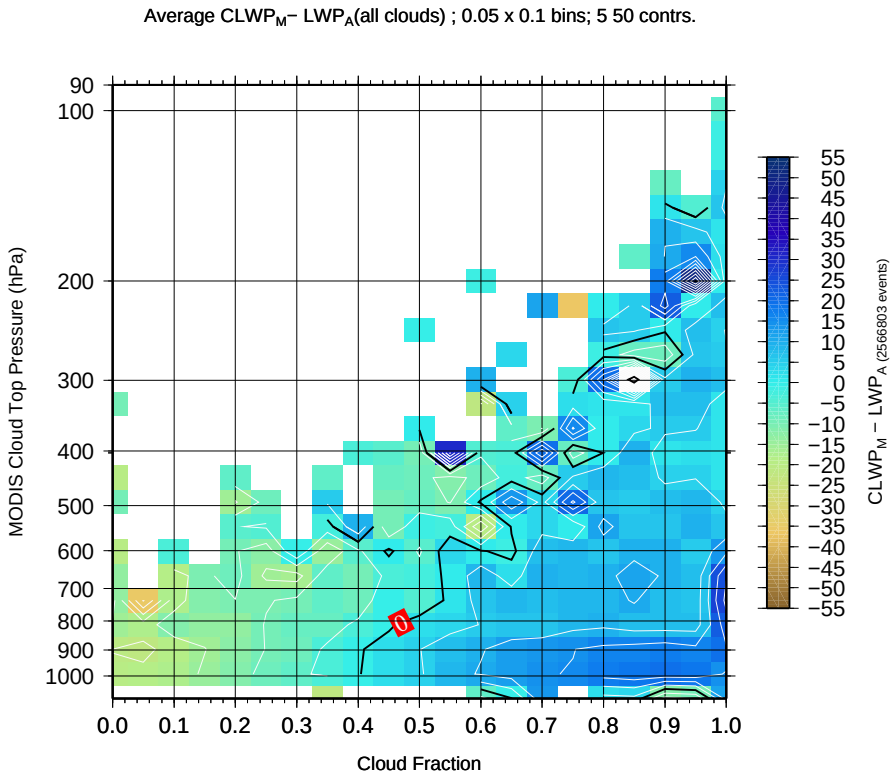

Fig. 5. ΔCLWP as a function of CTP and averaged CF for all clouds within each 0.25°×0.25° bin. The zero-difference contour line is black.

ACPD
9, 3367–3399, 2009

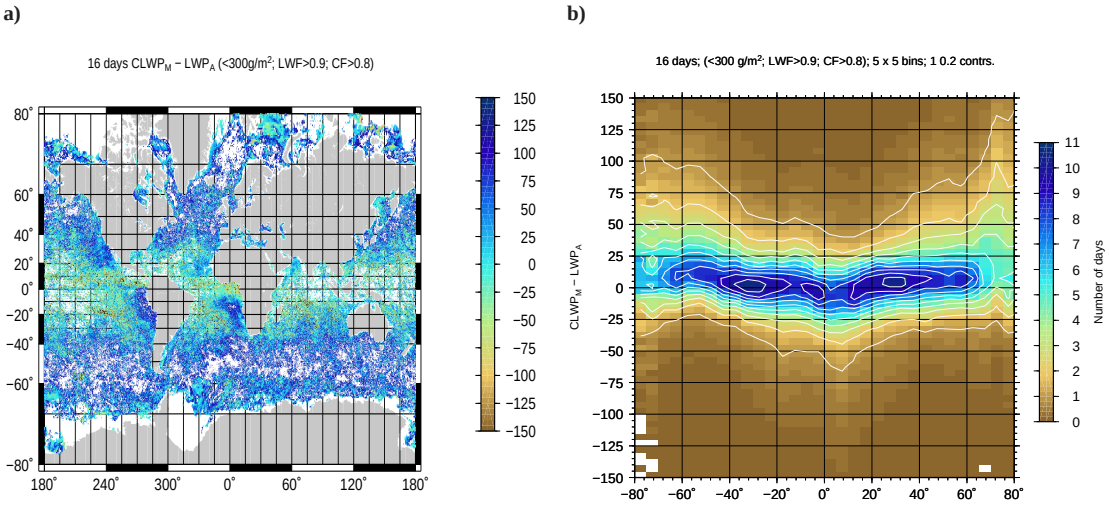

Fig. 6. (a) Map of average ΔCLWP for thin clouds on overcast locations (CF>0.8) where both instruments report less than 300 g m^{-2}; **(b)** frequency of occurrence of ΔCLWP by latitude.

ACPD
9, 3367–3399, 2009

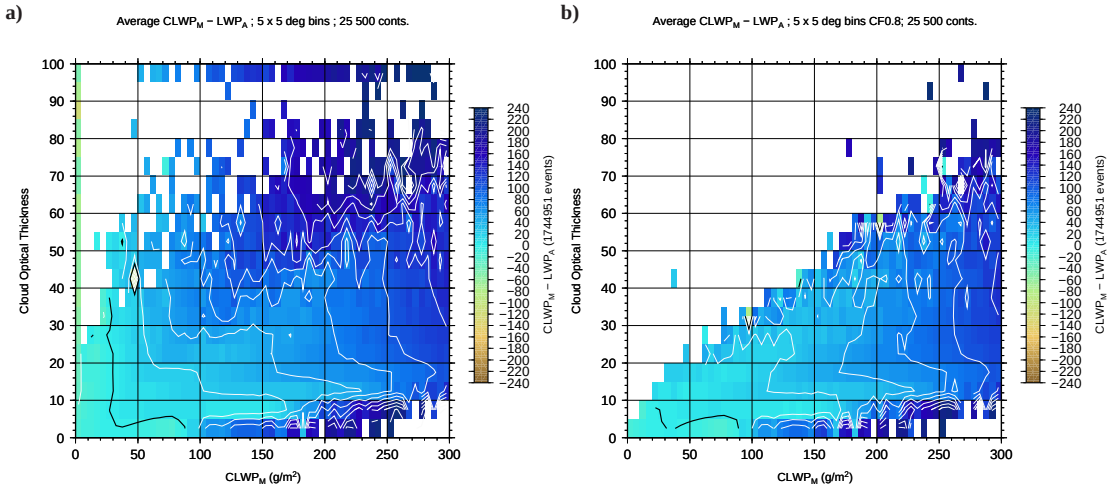

Fig. 7. ΔCLWP as a function of $CLWP_M$ and τ_c for **(a)** thin cloud (LWP<300 g m^{-2}) and **(b)** for overcast scenes (CF>0.8). The black contour line marks ΔCLWP=0. Thin white contours are each 25 g m^{-2}.

ACPD
9, 3367–3399, 2009

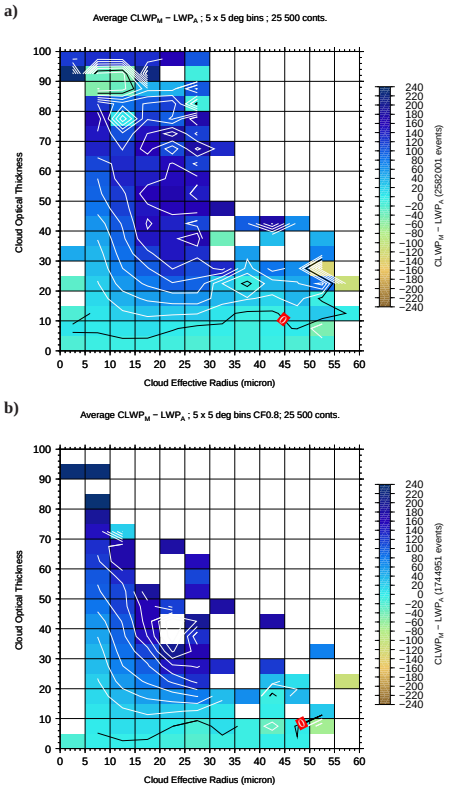

Fig. 8. ΔCLWP as a function of r_{eff}, and τ_c in thin cloud scenes with LWF>0.9. White contours mark 25 g m^{-2} increments and black marks the 0 g m^{-2} contour. **(a)** is for all clouds, and **(b)** for CF>0.8.

ACPD
9, 3367–3399, 2009

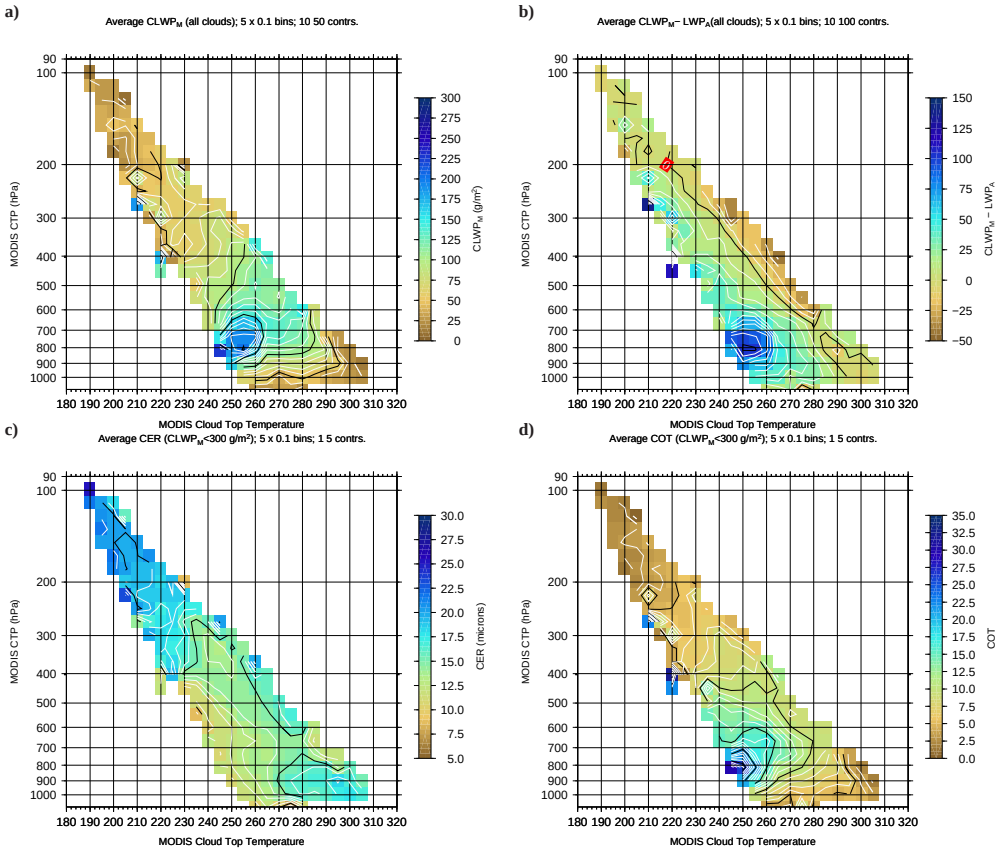

Fig. 9. **(a)** Average $CLWP_M$ for all clouds as a function of CTT and CTP; **(b)** ΔCLWP as a function of the average MODIS CTT and CTP within each cell. The zero difference contour line is shown in black; **(c)** r_{eff} as a function of CTT and CTP for thin clouds; **(d)** same as (c) but for τ_c.

ACPD
9, 3367–3399, 2009

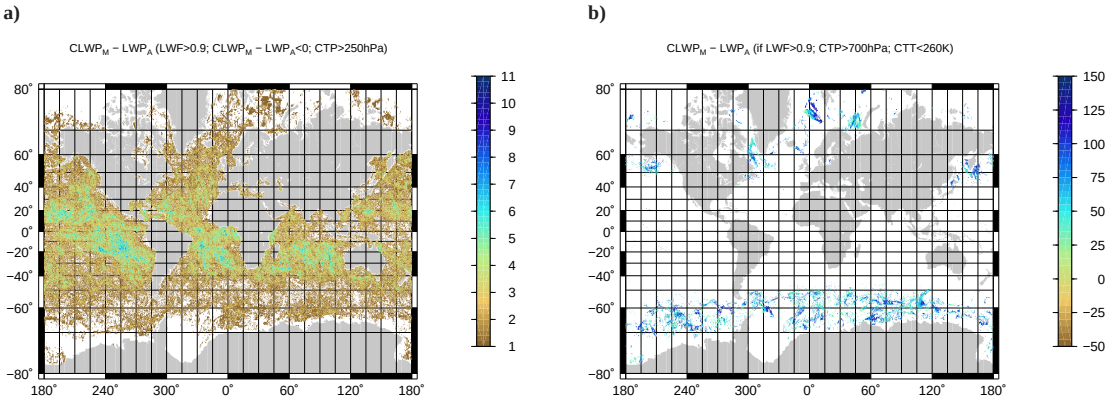

Fig. 10. **(a)** Number of days when $LWP_A > LWP_M$ for CTP>250 hPa. **(b)** ΔCLWP for clouds between 950–600 hPa limited to ΔCLWP>20 g m^{-2}.

ACPD
9, 3367–3399, 2009